

Article

Process Automation and Control Strategy by Quality-by-Design in Total Continuous mRNA Manufacturing Platforms

Axel Schmidt , Heribert Helgers, Florian Lukas Vetter, Steffen Zobel-Roos, Alina Hengelbrock 
and Jochen Strube *

Institute for Separation and Process Technology, Clausthal University of Technology, Leibnizstr. 15,
38678 Clausthal-Zellerfeld, Germany

* Correspondence: strube@itv.tu-clausthal.de

Abstract: Vaccine supply has a bottleneck in manufacturing capacity due to operation personnel and chemicals needed. Assessment of existing mRNA (messenger ribonucleic acid) vaccine processing show needs for continuous manufacturing processes. This is enabled by strict application of the regulatory demanded quality by design process based on digital twins, process analytical technology, and control automation strategies in order to improve process transfer for manufacturing capacity, reduction out-of-specification batch failures, qualified personnel training and number, optimal utilization of buffers and chemicals as well as speed-up of product release. In this work, process control concepts, which are necessary for achieving autonomous, continuous manufacturing, for mRNA manufacturing are explained and proven to be ready for industrialization. The application of the process control strategies developed in this work enable the previously pointed out benefits. By switching from batch-wise to continuous mRNA production as was shown in previous work, which was the base for this study, a potential cost reduction by a factor 5 (i.e., from EUR 0.380 per dose to EUR 0.085 per dose) is achievable. Mainly, based on reduction of personnel (factor 30) and consumable (factor 7.5) per campaign due to the significant share of raw materials in the manufacturing costs (74–97). Future research focus following this work may be on model-based predictive control to gain further optimization potential of potential batch failure and out of specification (OOS) number reduction.

Keywords: process automation; process control; digital twin; PAT; QbD



Citation: Schmidt, A.; Helgers, H.; Vetter, F.L.; Zobel-Roos, S.; Hengelbrock, A.; Strube, J. Process Automation and Control Strategy by Quality-by-Design in Total Continuous mRNA Manufacturing Platforms. *Processes* **2022**, *10*, 1783. <https://doi.org/10.3390/pr10091783>

Academic Editor: Alina Pyka-Pajak

Received: 4 August 2022

Accepted: 27 August 2022

Published: 5 September 2022

Publisher's Note: MDPI stays neutral with regard to jurisdictional claims in published maps and institutional affiliations.



Copyright: © 2022 by the authors. Licensee MDPI, Basel, Switzerland. This article is an open access article distributed under the terms and conditions of the Creative Commons Attribution (CC BY) license (<https://creativecommons.org/licenses/by/4.0/>).

1. Introduction

Messenger ribonucleic acid (mRNA)-based vaccines and treatments have demonstrated their potential during the international COVID-19 (coronavirus disease 2019) pandemic containment effort. Compared to traditional and established technologies, e.g., inactivated viruses, spike proteins, and AV (adenovirus) based vectors, mRNA-based vaccines have shown higher long-term efficacy with reduced side effects. The worldwide acceptance for this drug type was the necessary catalyst to open the way for further indications, such as prophylactic vaccination against other diseases, oncology, and molecular therapies.

1.1. State-of-the-Art in mRNA Manufacturing

The manufacturing process of mRNA starts with template DNA (deoxyribonucleic acid) that contains the genetic code for the respective protein. Cell-free manufactured DNA is feasible [1,2], state-of-the-art is still plasmid manufacturing by *E. coli* fermentation followed by purification and linearization [3]. The linearized DNA is used as a template in the *in vitro* transcription step. Often transcription and capping are separate process steps; however, nowadays co-transcriptional capping is regularly applied [4].

There are a wide variety of different separation technologies and overall purification strategies published in the literature (Figure 1). Although the major manufacturing steps of

transcription, purification, and final encapsulation into lipid nanoparticles are similar for the mRNA vaccines on the market and in development, the overall purification strategy and unit operations that are applied are not standardized [5,6].

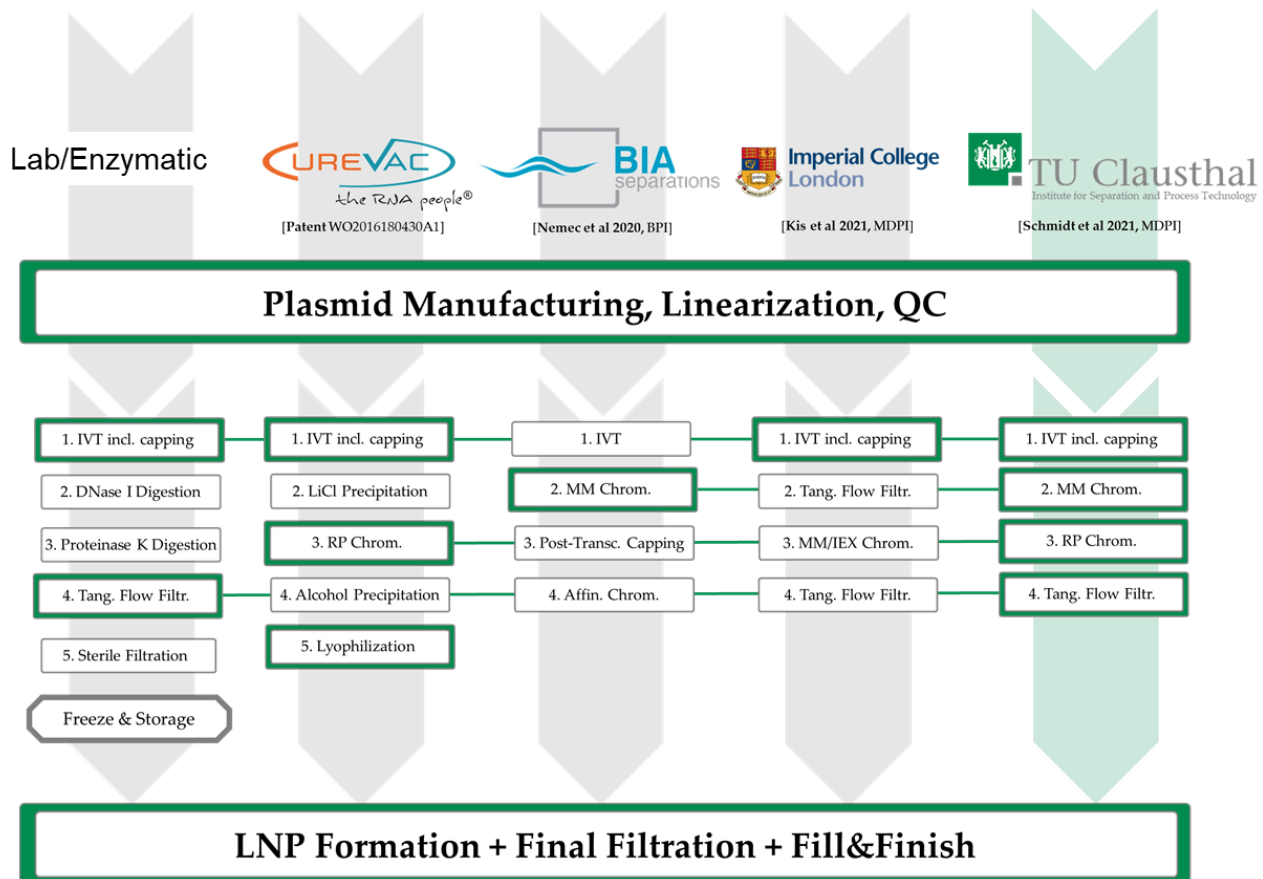


Figure 1. Main process phases in mRNA vaccine manufacturing. Plasmid manufacturing by *E. coli* fermentation followed by purification and linearization, followed by in vitro transcription, capping, and formulation including encapsulation of mRNA in LNP.

Reversed phase chromatography mode is essential for final product quality purity attributes in order to enrich PolyA-mRNA as target component and side components adenosine and polymerase above 99.9% purity [7]. In addition, a priori for safety reasons an orthogonal purification method based on mixed-mode chromatography before the final reversed-phased (RP) step may be a logical choice to improve RP polishing performance [8,9].

RP chromatography purification task is dedicated to gain final polishing of the single-strain mRNA end product from adenosine and polymerase above 99.9% purity. In RP mode, the product is bound by differing polarity and all those side components are eluted, therefore a periodic counter current operation is the set-up of choice within all available continuous chromatography modes [10,11].

Whereas a preceding mixed-mode chromatography step has the objective to purify the product fraction by about 99%, in order to relieve the RP separation task [8].

The corresponding process control simulation study is described in detail in [12] as it would expand the scope of this total process overview too much into continuous chromatography specific details. The results may be summarized as the conclusion that any industrialization of the proposed automation concept is straight forward based on standard PID controller positioning and configuration [12,13]

1.2. Quality Assurance, Quality Control and Quality-by-Design (QbD)

QbD-based process development is established as the gold standard for new pharmaceutical products, such as virus-like particles, plasmid DNA, fragments, etc., because it ensures quality over the entire life cycle and allows process changes even after approval if there is potential for optimization, and because there are no comparable platform processes as for monoclonal antibodies [14–17].

FDA (U.S. Food and Drug Administration), EMA (European Medicinal Agency), ICH (International Council for Harmonization of Technical Requirements for Pharmaceuticals for Human Use), and several industry working groups have launched initiatives and published a number of guidance documents, the most prominent example being QbD-related ICH Q8 to Q13 [18–21].

However, the application of QbD principles to process development requires a validated design space that guarantees consistent quality, which can be developed either through experimentation or process understanding. Therefore, there is a need for digital twins in process development as well.

At the beginning of a QbD-based process development, a quality target product profile (QTPP) must be derived. This is necessary to define what is crucial for the product quality. Characteristics for biologics are e.g., sterility and purity, but also certain therapeutic effects, bioactivity and dosage. Depending on the QTPP, critical quality attributes (CQAs) have to be defined, i.e., a property or characteristic that ensures the desired product quality when controlled within a defined limit, range, or distribution [15,22].

Following the QbD philosophy, CQAs are not static but dynamic and need to be updated during the life cycle of products when newly developed product and process knowledge suggests this. CQAs guide further process development and are derived through risk management and experimentation. Risk assessment is part of risk management and should be performed early in process development. Its purpose is to establish known and hypothetical links between material, equipment, and process parameters to CQAs. In doing so, it establishes the framework for further process design. Common tools for this, which are also suggested by FDA, EMA, PDA, and ICH, are the preparation of Ishikawa diagrams, also called fishbone diagrams, and the performance of a failure mode and effects analysis (FMEA) [19]. The Ishikawa diagram mainly summarizes different groups of effects, e.g., material properties, plant design and process parameters, which can cause a risk for certain CQAs, such as yield, purity, or processability in general. The major branches are broken down into minor branches that show more detailed causality between cause and risk. The level of detail depends only on the prior knowledge gathered by the process development team. This diagram may already show critical process parameters (CPPs) that need to be kept within a certain range during the process and therefore should be part of a process management strategy and may need to be investigated further.

Predictive process models as digital twins are the key tools for a quantitatively defined and knowledge-based process optimum. They accelerate process development and generate process knowledge at the same time. They help reduce experimental effort and their validity does not end in the initial approved design space due to their physicochemical nature. Of course, any model to be used in this way must be at least as accurate and precise as the particular experiments it is intended to replace [17,23]. One-factor-at-a-time studies can show which parameters should be included for multivariate studies based on their impact. By applying DoE (design-of-experiments) principles, an experimental design can be created to characterize the design space.

1.3. Process-Analytical-Technology (PAT) and Process Control Strategies

Continuous biomanufacturing studies have proven the potential to maintain high product quality and timely, reliable supply of biologics [24–28]. The continuous production suggests to automate the process [29,30]. Even if continuous operation may be comparably short, with about 2 weeks to 2 months when compared to bulk and petro chemicals operation times of up to several months. Autonomous operation reduces product quality

variance and keeps the operation state constant around an optimum by advanced process control strategies [31]. Benefits are reduced operation costs, reduction of manufacturing [32], and significant QA (quality-assurance) cost reduction by real-time-release-testing (RTRT) [33]. The basis of advanced-process-control (APC) are models either artificial neural networks (ANN), rigorous or hybrid [33,34]. Digital twins based on process models which need to be distinctively validated for regulatory decisions are combined with PAT via statistical-based data evaluation toward process control strategies.

The digital twin in continuous biologics manufacturing will require key technologies and concepts such as PAT and QbD [35–37]. In the case of mRNA vaccine production (see Figure 2), lengthy quality controls occur first when controlling the linearized DNA, which is the starting material in the production of the actual mRNA drug, and secondly they are necessary before the purified mRNA drug can be encapsulated. This results in holding times of up to several weeks [32]. PAT is a necessary key-enabling technology for continuous biomanufacturing. Most (spectroscopic) sensors are based on chemometric calculations (e.g., partial least square regression, principal component analysis), which are already widely used in the literature. Additionally, there are model-based sensors, which can be based on mass and/or energy balances as well as (extended) Kalman filters, whose implementation are more time-consuming. However, the last-mentioned sensors provide an extended process understanding, as they can be based on physicochemical effects [28,38–40].

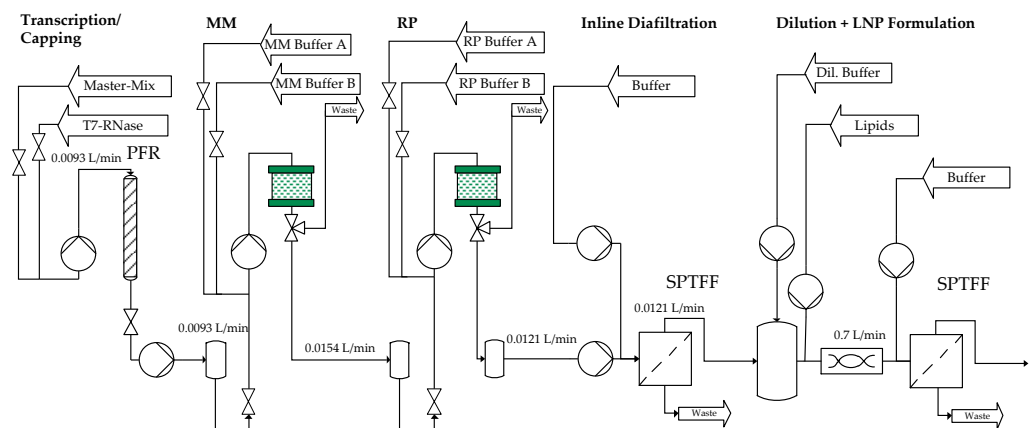


Figure 2. Process overview of continuous mRNA manufacturing.

In terms of automation digital twins in continuous biomanufacturing rely on online process data that updates the information fed into the process models in real-time [28,41–44]. Besides simple process parameters such as pressure, conductivity, pH, temperature, etc., concentration of the target component and main impurities are necessary to ensure that the information gathered from the digital twin are reliable. Spectroscopic technologies such as Raman, Fourier-transform-infrared (FTIR), UV-vis, fluorescence, and circular dichroism have been demonstrated to be suitable detection methods for a variety of biologics manufacturing processes.

2. Materials and Methods

2.1. In Vitro Transcription

The equations describing the reaction kinetics of in vitro transcription were taken from the literature. They are based on Michaelis–Menten kinetics, which additionally consider inhibition by by-products [45]. The maximum reaction rate (r_{max}) is a function of the turnover rate (k_{eff}) and the enzyme concentration (c_e).

$$r_{max} = k_{eff} \cdot c_e \quad (1)$$

The dependency of the enzyme activity (act_i) on temperature (act_{Temp}), pH (act_{pH}), and magnesium chloride concentration (act_{MgCl_2}) can be described using sigmoidal functions based on data from the literature [46].

$$act_i = \left(Y_{LS,i} + \frac{Y_{mid,i} - Y_{LS,i}}{1 + e^{-K_{LS} \cdot (X - r_{max,low,i})}} \right) \cdot \left(1 + \frac{\frac{Y_{RS,i} - 1}{Y_{mid,i}}}{1 + e^{-K_{RS,i} \cdot (X - r_{max,high,i})}} \right) \quad (2)$$

X is either the temperature, the pH, or the magnesium chloride concentration, depending on which parameter the dependency of the activity is to be described by means of the sigmoidal function given in Equation (2).

The change in pH during the reaction is described with the aid of the Henderson-Hasselbalch equation. This describes the pH of buffer systems by considering the negative decadic logarithm of the acid constant (pK_a) as well as the acid (c_{HA}) and the conjugated base concentration (c_{A^-}) [47].

$$pH = pK_a + \log \left(\frac{c_{A^-}}{c_{HA}} \right) \quad (3)$$

The reaction rate (r) of in vitro transcription results in [45]:

$$r = \frac{act_{pH} \cdot act_{Temp} \cdot act_{MgCl_2} \cdot r_{max}}{1 + \sum_{j=1}^N \frac{K_{M,NTP,j}}{c_{NTP,j}} \cdot \left(1 + \frac{c_{PPi}}{K_{I,PPi}} + \sum_{i=1}^N \frac{c_{NTP,i}}{K_{I,PPi}} \right) + \frac{K_{M,DNA}}{c_{DNA}} \cdot \left[1 + \frac{K_G}{c_{GTP}} \cdot \left(1 + \frac{c_{PPi}}{K_{I,PPi}} + \sum_{i=1}^{N-1} \frac{c_{NTP,i}}{K_{I,NTP,i}} \right) \right]} \cdot \frac{c_{cap}}{c_{cap} + K_{M,cap}} \cdot \frac{c_{mRNA}}{c_{mRNA} + K_{M,mRNA}} \quad (4)$$

It describes the influence of the concentrations of nucleotides (c_{NTP}), pyrophosphate (c_{PPi}), promoter (c_{DNA}), cap analog (c_{cap}), and mRNA (c_{mRNA}), as well as inhibition by competition of the nucleoside tri phosphates ($K_{I,NTP}$), excluding GTP, and pyrophosphate ($K_{I,PPi}$). Furthermore, it includes the Monod constants of the nucleotides ($K_{M,NTP}$), promoter ($K_{M,DNA}$), cap analog ($K_{M,cap}$), and mRNA ($K_{M,mRNA}$). In addition, there is the dissociation constant of the initial binding of GTP (K_G), whereas (c_{GTP}) represents the guanosine triphosphate concentration. The equation in the square brackets in the denominator describes the initiation process of in vitro transcription. This consists of binding of the promoter to the enzyme.

The change in concentration due to the reaction of the nucleotides (f_i describes the proportion of the nucleotide i in the mRNA) and also the by-product PPi is dependent on the length of the mRNA n_{mRNA} [45]:

$$\frac{dc_{NTP,i,react}}{dt} = -f_i \cdot n_{mRNA} \cdot r \quad (5)$$

$$\frac{dc_{PPi,react}}{dt} = (n_{mRNA} - 1) \cdot r \quad (6)$$

The reaction takes place in a plug flow reactor (PFR), which is described using an axial dispersion model. This gives the total concentration change via the sum of the concentration change over the reactor length resulting from convection due to the fluid velocity u , the concentration change due to dispersion analogous to Fick's law, where the parameter D_{ax} describes the extent of back-mixing, and the concentration change due to the reaction (r) [48].

$$\frac{\partial c_i}{\partial t} = -u \cdot \frac{\partial c_i}{\partial z} + D_{ax} \cdot \frac{\partial^2 c_i}{\partial z^2} + r \quad (7)$$

The differential equations can be solved by introducing the Danckwerts boundary conditions for the closed-closed vessel [49,50].

$$\frac{\partial c(z=L)}{\partial z} = 0 \quad (8)$$

$$D_{ax} \cdot \frac{\partial c(z=0)}{\partial z} = u \cdot (c(z=0) - c_{in}) \quad (9)$$

2.2. Single-Pass Tangential Flow Filtration

Characterization and control studies for inline diafiltration by SPTFF (single-pass-tangential-flow-filtration) are based on a validated process model previously developed and published by Huter et al. [51–53] and Thiess et al. [54,55]. The permeate volume flow in ultrafiltration is in general dependent on the permeability L_p , the total membrane area A_m , as well as the driving force DF:

$$\dot{V}_P = L_p \cdot DF \cdot A_m = J_V \cdot A_m \quad (10)$$

Driving force reducing effects such as osmotic pressure P_{Osm} can be calculated by correlations based on the solute concentration on the membrane surface c_m .

$$DF = TMP - P_{Osm}(c_m) \quad (11)$$

The transmembrane flux decline by concentration polarization is then described by Equation (10), first introduced by Michaels [56]:

$$J_V = k_f \cdot \ln\left(\frac{c_m}{c_b}\right) \quad (12)$$

The permeability of the membrane is given by:

$$L_p = \frac{1}{\eta \cdot R_m} \quad (13)$$

So that the total transmembrane flux can be calculated as:

$$\dot{V}_P = \frac{TMP - P_{osm}}{\eta \cdot R_m} \cdot A_m \quad (14)$$

Final buffer exchange BE and the volumetric concentration factor VCF are defined as:

$$BE = \frac{c_{SC,in}}{c_{SC,out}} \times 100 \quad (15)$$

$$VCF = \frac{c_{TC,in}}{c_{TC,out}} \quad (16)$$

2.3. Lipid-Nanoparticle Formation

The LNP formulation is carried out in a T-mixer, with the mRNA in an aqueous buffer at pH 4. The lipids, which are composed of an ionizable lipid ($c_{ion.lipid}$), a helper lipid ($c_{helper\ lipid}$), cholesterol ($c_{cholesterol}$), and a PEG lipid ($c_{PEG\ lipid}$), are present in an organic solvent phase such as ethanol. The phases are mixed in a ratio of 3:1 (aqueous:organic solvent phase).

The pH value obtained when the two phases are mixed can be calculated using the Henderson–Hasselbalch Equation (see Equation (3)).

It is assumed that the reaction follows the following kinetics with r as the reaction rate.

$$r = k \cdot c_{mRNA} \cdot c_{ion.lipid} \cdot c_{helper\ lipid} \cdot c_{cholesterol} \cdot c_{PEG\ lipid} \quad (17)$$

The change in concentration due to the reaction for the mRNA and lipids is calculated using Equation (11).

$$\frac{dc_{i,react}}{dt} = -f_i \cdot r \quad (18)$$

The proportions of lipids and mRNA (f_i) in an LNP and the rate constant were taken from the literature. The pH dependence of the rate constant (k) can be described as follows [57–59].

$$k = \frac{k_1 \cdot K_a + k_2 \cdot c_{H_3O^+}}{K_a + c_{H_3O^+}} \quad (19)$$

The rate constant depends on the rate constants (k_1 and k_2) of the forward and reverse reactions of ionization as well as the oxonium ion concentration ($c_{H_3O^+}$) and the acid constant of the ionizable lipid (K_a).

The LNP formulation in the T-mixer is represented by the axial dispersion model with Danckwerts boundary conditions (see in vitro transcription). The modeling of the subsequent buffer exchange is analogous to SPTFF as described in Section 2.2.

2.4. Impact Assessment and Statistical Analysis

In order to plan process characterization and control studies, a risk assessment approach as presented in the A-mab case study by the CMC (chemical, manufacturing and control) working group is chosen. The workflow to select which parameters are included in OFAT (one-factor-a-time), DoE, and finally control studies consists of the following steps:

1. Identification of parameters for OFAT studies in Ishikawa analysis;
2. Main effect ranking based on impact attributes after OFAT studies and assessment of possible impact of interaction;
3. Calculation of severity scores and execution of derived statistical experimental designs;
4. Analysis of study results to quantify parameter effect strength, identify CPP, KPP (key process parameter), and process optima as well as to define design space, control space, and PAR (proven acceptable range).

The determined value for impact and interaction is then multiplied and based on the scores given in Table 1, either a univariate or multivariate examination on the parameter is performed. Variables with a score of ≤ 2 are not studied, those with scores 4–8 can be studied univariately or multivariately and those with higher scores are studied multivariately. The decision of whether variables with 4–8 scores have to be studied univariately or multivariately must be properly justified.

Table 1. Ratings for the impact and interaction assessment of potential variables on the process attributes and the CQAs.

Impact	Critical Quality Attribute (CQA)	Process Attribute
No Impact/Interaction	1	1
Minor Impact/Interaction	4	2
Major Impact/Interaction	8	4

The resulting multivariate study is the design space for the chromatographic process. The endpoints of this multidimensional space are modelled in a full-factorial DoE and the resulting design space can be evaluated statistically.

2.5. Process Control Parameter Determination

Controller design and parameter determination for all PID were done according to the Ziegler–Nichols [60,61] and Chien–Hrones–Reswick tuning method [61,62].

3. Results

3.1. Risk Assessment and Impact Ranking

3.1.1. Ishikawa Analysis

In Vitro Transcription

To qualitatively determine the risks to the space-time yield (STY) of capped mRNA in in vitro transcription, a risk analysis was performed using an Ishikawa diagram (see

Figure 3). In addition to variables that are not easily quantifiable, such as risk factors affecting staff, and product properties that cannot be influenced, such as mRNA sequence, the materials used as well as the equipment and some process parameters have an impact on STY. In particular, parameters that have an impact on kinetics, enzyme stability, and hydrodynamics pose a major risk to the critical process attribute (CQA) of STY. These include enzyme and template concentration, the amount of nucleotide and cap analog used, the ratio of reactor length to diameter, and process parameters such as temperature, pH, and volume flow rate. Accordingly, these risk factors are quantified using one factor at a time (OFAT) analysis.

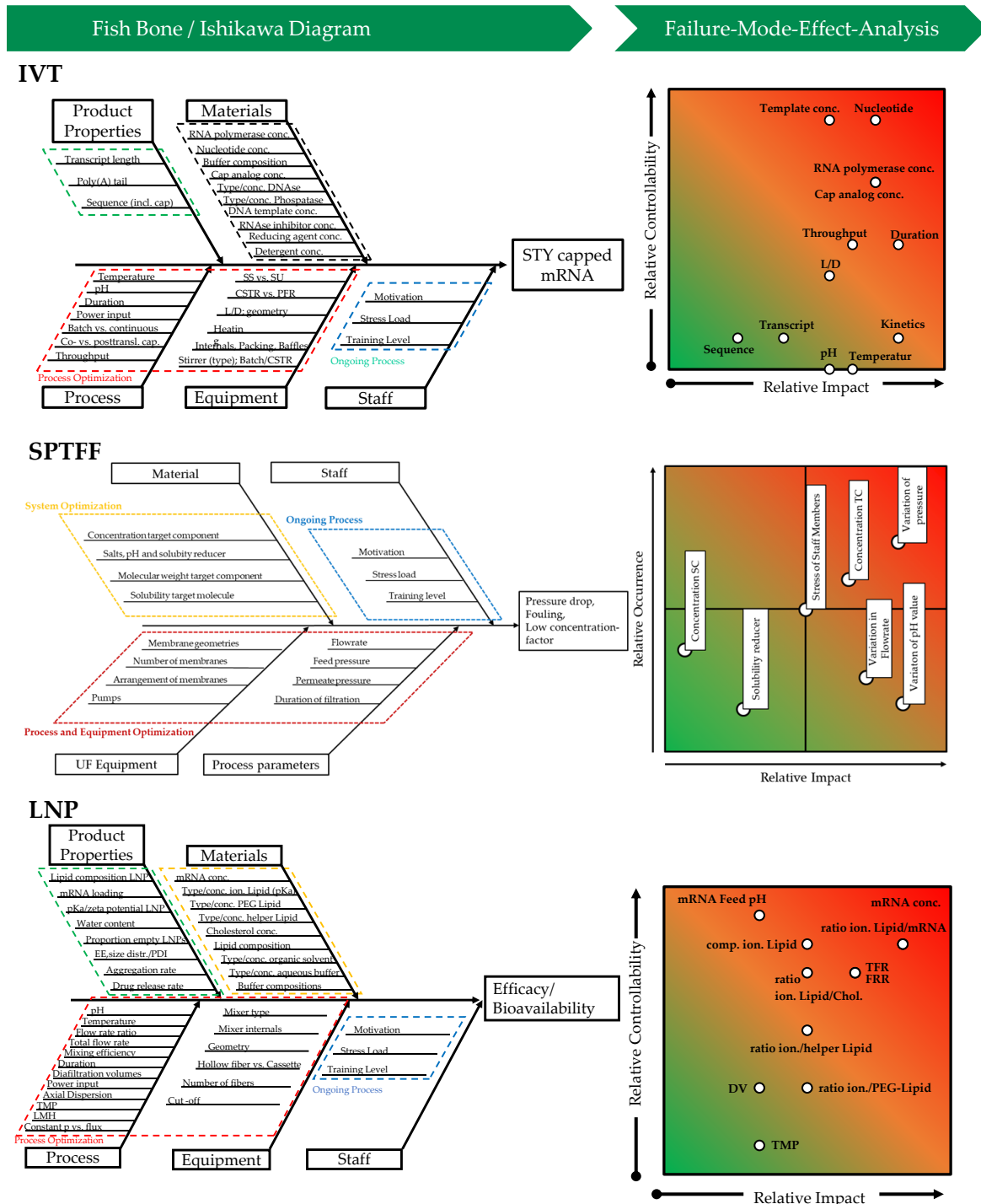


Figure 3. Ishikawa and graphical impact ranking analysis.

Inline Diafiltration by SPTFF

In case of continuous ultrafiltration, the process is mainly influenced by pressure and flowrate. While higher flow rates increase the throughput, they also lead to higher feed pressures and pressure losses. Furthermore, the used equipment sets the boundaries for possible throughput and the used membrane configurations have an impact on the feed pressure resulting from the feed flow. Besides this process optimization, fluctuating process parameter or other solubility reducer can affect the buffer exchange efficiency, e.g., by increased membrane resistance. This can be the result of fouling.

LNP Formation

The risk factors in the LNP formulation are qualitatively represented in an Ishikawa diagram (see Figure 3). Both personnel, especially their training levels, stress load, and motivation, and product characteristics such as lipid composition and mRNA content are risks in LNP formulation. These factors are either difficult to quantify or are influenced by the materials, equipment, and process parameters used. Consequently, risks such as substrate amounts, mRNA concentration, and factors affecting hydrodynamics such as volume flow rate and volume flow ratio will be quantified using OFAT. Furthermore, the number of diafiltration volumes and the transmembrane pressure (TMP) will be considered.

3.1.2. One-Factor-A-Time Studies and Impact Ranking

In Vitro Transcription

According to OFAT analysis, the concentrations of enzyme, nucleotides, cap analog, and template used have barely any effect on the space-time yield if only one parameter is currently fluctuating (see Table 2). For the template concentration, this was to be expected because it only minimally affects enzyme kinetics and is used in excess because it is cheap. In contrast, the kinetics are strongly influenced by the enzyme and substrate concentrations. This primarily comes into account in the interactions of the parameters with each other, which is why these variables are investigated multivariately in the statistical experimental design. Furthermore, the enzyme kinetics depend on the temperature and the pH value. The latter decreases in the progress of the reaction, which is why it is investigated multivariately, whereas the temperature is easily controllable in the process and consequently enters univariately. The volumetric flow rate, which is crucial for back-mixing, flow regime, and residence time, among others, has a large main effect on the STY. In addition, strong interactions with the other parameters are expected, which is why the volume flow rate is investigated multivariately.

Inline Diafiltration by SPTFF

In inline diafiltration, the most important CQA is to achieve a necessary degree of desalination by buffer exchange before formulation. As a process attribute, the volumetric concentration factor must be kept within process—technically reasonable—but also economic limits. Too high a concentration after diafiltration unnecessarily increases and thus complicates dilution directly before LNP formation. However, it is even more important not to let the concentration in the DF drop too much, so that an optimal concentration before formulation is still possible by dilution.

Within the limits studied, most of the process parameters (VF_{in}, TMP), module parameters (membrane permeability, diameter, length and number of fibers), as well as feed solution viscosity are of significance for the degree of desalting (see Table 2). Since after MMC and RPC the product is of high purity, no decisive influence of the component concentrations on the desalting efficiency due to e.g., gel layer formation is to be expected, which is in line with the experience of similar DF operations. The volumetric concentration factor shows a more differentiated picture of the effect strengths. Thus, the main process variables TMP and volumetric flow rate of the exchange buffer are again significant. The other parameters (feed and module properties) are less so. Due to the previously defined severity limits for the planning of the investigation studies, all parameters are included in

the multivariate investigation, whereby TMP and volume flow of the exchange buffer can now be expected as the strongest effects from the OFAT (40 simulations) study. This results in 1025 simulations for a full factorial investigation and a center point.

Table 2. Final impact assessment after OFAT studies and overview of main effect, interaction, and overall severity score. Green: no impact. Orange: Minor impact. Red: major impact.

In Vitro Transcription	Factor	Main Effect CQA (purity)	Main Effect PA (STY)	Highest Main Effect Score	Interaction CQA (purity)	Interaction PA (STY)	Highest Interaction Score	Severity
	T7 conc	1	1	1	4	4	4	4
NTP conc	8	4	8	8	4	8	64	
Cap-analog conc	8	1	8	8	2	8	64	
Template conc	1	1	1	1	2	2	2	
Temp	8	4	8	4	1	4	32	
pH	8	4	8	1	1	4	32	
VF tot	1	4	4	8	4	8	32	
L/D	1	1	1	1	2	2	2	
Inline Diafiltration SP ^{TFF}	Factor	Main Effect CQA (BE)	Main Effect PA (VCF)	Highest Main Effect Score	Interaction CQA (BE)	Interaction PA (VCF)	Highest Interaction Score	Severity
	VF Feed	8	2	8	4	2	4	32
mRNA conc	2	2	1	2	2	2	2	
SC conc	2	2	1	2	2	2	2	
Viscosity	8	4	8	2	2	2	16	
Fiber Diameter	8	4	8	4	4	4	32	
Fiber Length	8	4	8	4	4	4	32	
Fiber Count	8	4	8	8	8	8	64	
R _m	8	4	8	2	2	2	16	
TMP	8	8	8	8	8	8	64	
VF EB	4	8	8	8	8	8	32	
Lipid-Nanoparticle Formation	Factor	Main Effect CQA (EE)	Main Effect PA (c _{LNP})	Highest Main Effect Score	Interaction CQA (EE)	Interaction PA (c _{LNP})	Highest Interaction Score	Severity
	mRNA conc	8	2	8	4	2	4	32
mRNA Feed pH	4	2	4	8	4	8	32	
WR Lipids:mRNA	8	4	8	4	4	4	32	
w% ionizable Lipid	8	4	8	4	4	4	32	
w/w ion./PEG-Lipid	8	4	8	2	2	2	16	
w/w ion./help Lipid	8	4	8	2	2	2	16	
w/w ion./Chol.	8	4	8	4	2	4	32	
VF tot	1	4	4	8	4	8	32	
v/v aq/EtOH	8	4	8	4	4	4	32	
DV	1	4	4	1	2	2	8	
TMP	1	4	4	1	1	1	4	

LNP Formation

In particular, the lipid composition, the mRNA concentration, the total volume flow, and the volume ratio of aqueous to organic solvent phase influence the LNP formulation. The lipid concentrations used and the amount of mRNA present significantly affect the reaction kinetics (see Table 2). In addition, the amount of helper lipids used is responsible for stability and that of the PEG lipid for inhibiting aggregate formation. Whereas the mRNA concentration and the amount of ionizable lipid additionally influence the encapsulation efficiency (EE). The adjusted volume flow rate determines the residence time as well as the hydrodynamics of the LNP formulation. Furthermore, interactions between these parameters are expected, which is why they are investigated multivariately in the statistical experimental design. Further risks are posed by the pH of the aqueous buffer and the diafiltration volumes used, which are also multivariately included in the DoE. Here, the pH plays an important role for ionization of the ionizable lipid and the diafiltration volumes are responsible for efficient buffer exchange for neutralization and quenching of the reaction. Only the TMP is studied univariately, since it has a minor influence on the process time as well as the blocking behavior and hardly any interactions are expected.

3.2. Multivariate Studies and Design Space Characterization

IVT

By reducing the *p*-value, the two-stage full factorial statistical experimental design, which corresponds to a total of approx. 8200 simulations substituting experiments, was evaluated and as Figure 4 shows, a good regression quality can be achieved with an R^2 of 0.9 and a *p*-value < 0.0001 even though there are a few clusters in the lower region. The biggest

influence on the space-time yield in in vitro transcription is the volume flow rate. This agrees with the results from the OFAT study. The nucleotide and enzyme concentrations and their interactions with each other and with the volume flow rate were identified as further significant factors. Consequently, the significance of these factors emerges only through their interactions, because if only one factor varies, the effect on STY is small (see Figure 4).

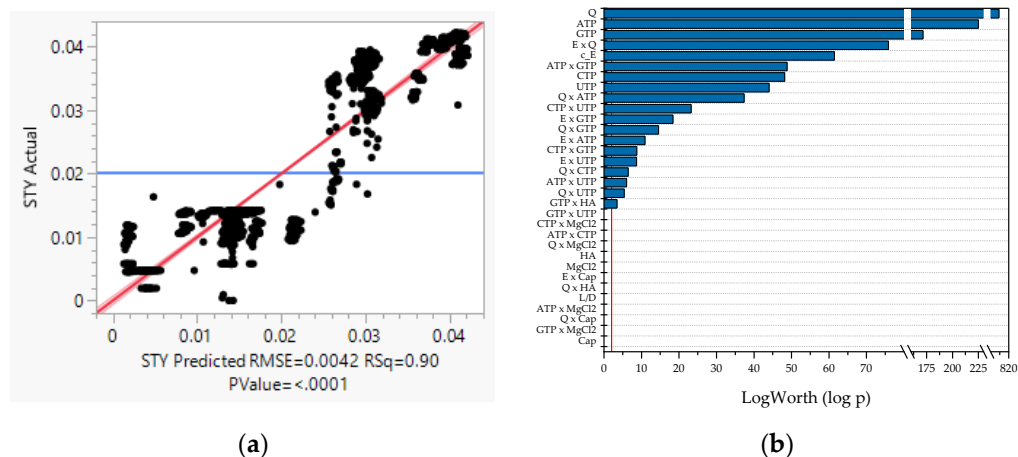


Figure 4. Regression and effect strengths IVT STY. (a) Actual-vs-predicted plot. (b) log-worth of effects.

In addition to the identification of significant factors influencing the space-time yield, a design space can be spanned by the statistical evaluation of the experimental design (see Figure 5). To maximize STY, the use of high nucleotide concentrations is necessary. Furthermore, the use of large amounts of enzymes and the establishment of a high volumetric flow rate is beneficial.

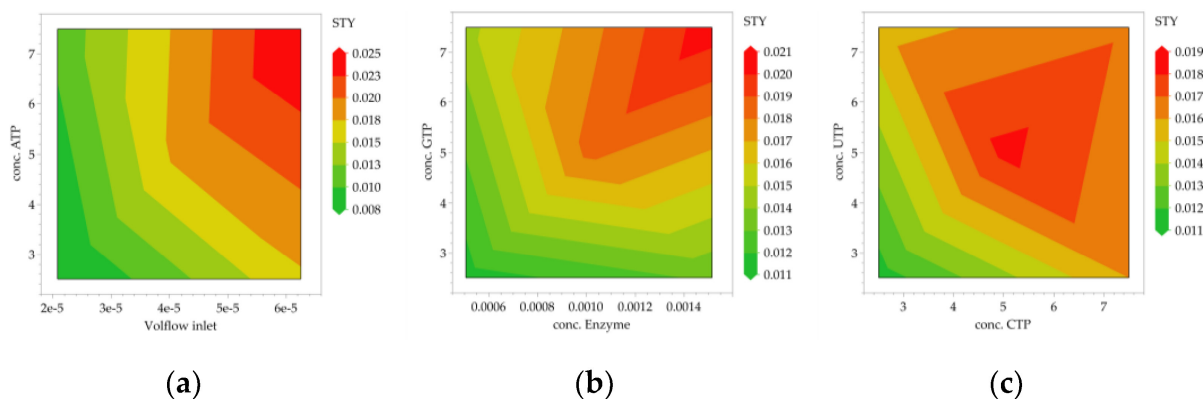


Figure 5. Contour plot IVT STY. (a) ATP concentration and volume flow inlet. (b) Concentration GTP and concentration enzyme. (c) Concentration UTP and concentration CTP.

Inline Diafiltration by SPTFF

The evaluation of the multivariate process characterization of the SPTFF is shown in Figure 6. The usual evaluation of DOE results via OLS (ordinary-least-squares) already shows a very good regression quality with an R^2 of 0.98. PLS (partial-least-squares) and a ANN were used additionally to demonstrate the different possibilities in the statistical evaluation. For ANN the size of training set was 970 and for validation 485. The p-value is smaller than 0.001, so the statistical conclusions can be considered robust. An evaluation by means of a neural network allows, moreover, an even better regression of the results with an R^2 of 0.99.

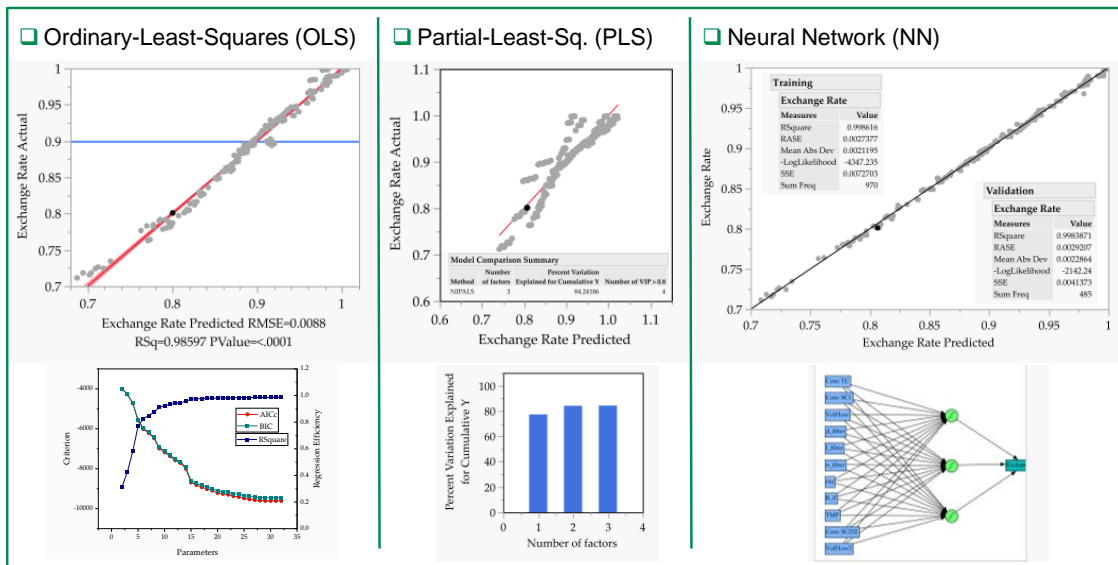


Figure 6. Comparison of regression efficiency and probability of OLS, PLS, and NN in SPTFF.

The analysis of the effects (Figure 7) shows for all three regression methods that the TMP and the volumetric flow rate of the exchange buffer are the most significant effects on the buffer exchange BE and the volumetric concentration factor VCF. While the OLS and PLS statements are very accessible via the log-p value (OLS) and the VIP score (PLS), respectively, the analysis of the effect sizes in the neural network is more difficult, and increases in complexity with the number of nodes and layers.

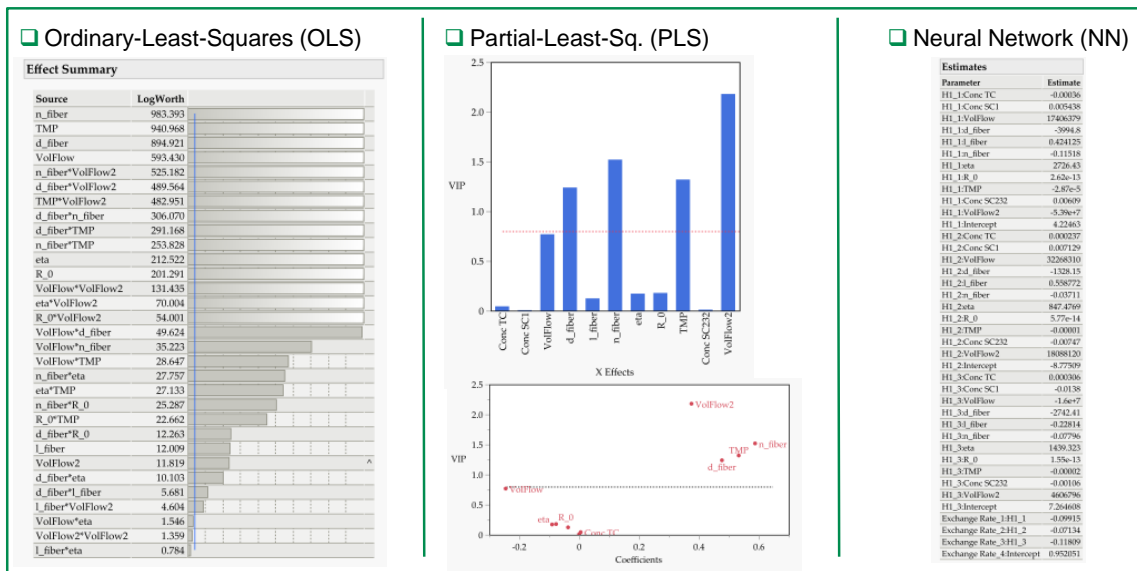


Figure 7. Comparison of possible effect analysis between OLS, PLS, and NN in SPTFF.

The design space from the OLS (see Figure 8) over the two critical process parameters buffer exchange flow rate and TMP shows that the optimum is at a TMP of 1.4 bar and a buffer exchange flow rate of 13 mL/min.

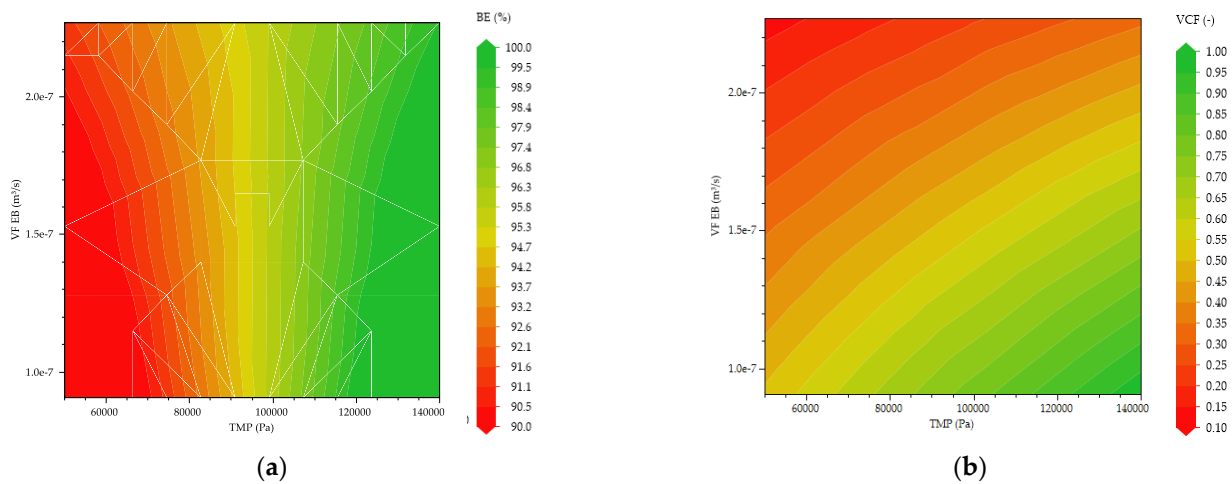


Figure 8. Contour plot for buffer exchange (left (a)) and volumetric concentration (right (b)) factor in SPTFF based on OLS-regression model.

Comparing the resulting optimizations (Figure 9) of OLS, PLS, and neural network, in principle similar curves can be seen for the two critical process parameters. However, the desirabilities differ between simple OLS and PLS or NN. Thus, the influence of the TMP is linearly positive for all three regressions, whereas PLS and NN are able to detect a nonlinear influence for the exchange buffer flow rate.

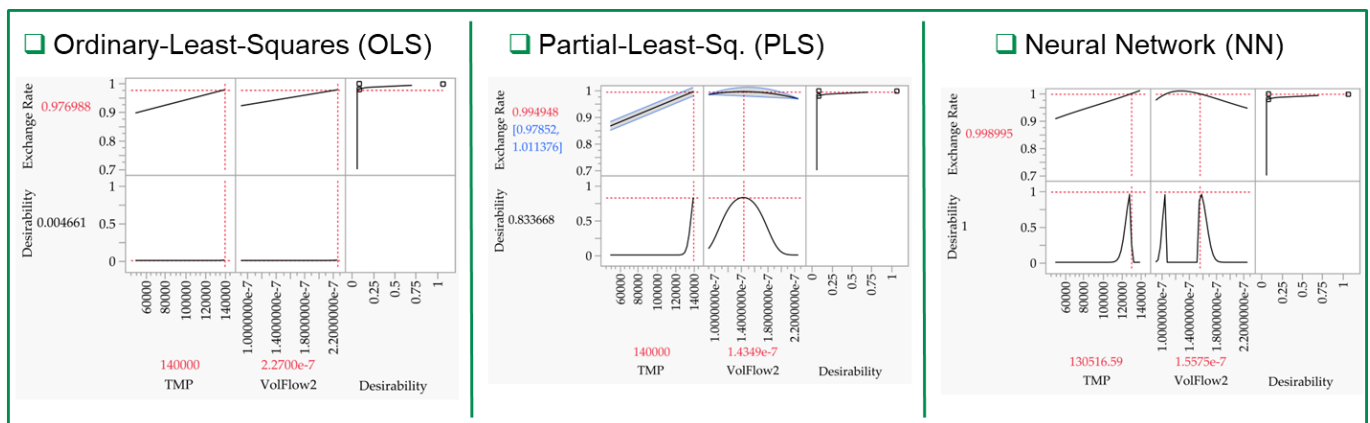


Figure 9. Comparison of optimization prediction by PLS, PLS, and NN regression.

LNP

The two-stage full factorial experimental design includes over 1000 simulations substituting experiments and was evaluated for the LNP formulation in terms of encapsulation efficiency (EE) and the resulting LNP concentration by reducing the p-value stepwise. The regression is sufficiently accurate for both target variables, with an R^2 of 0.81 for EE and 0.71 for LNP concentration, respectively (see Figure 10). For the EE, the mRNA concentration and the volume flows of the aqueous and organic phases, respectively, are particularly significant, as was already evident from the OFAT analysis. Moreover, in good agreement with the OFAT study is the influence of lipid concentrations and their interactions, as well as the single influence of pH on EE. Only the expected strong interactions of pH could not be observed.

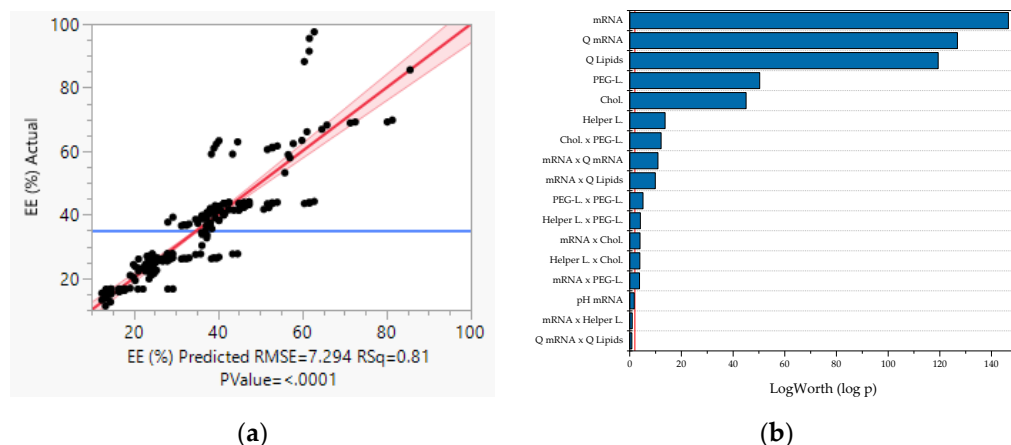


Figure 10. Regression and effect strengths LNP encapsulation efficiency. (a) Actual-vs-predicted plot. (b) log-worth of effects.

For the resulting LNP concentration, the volume fluxes of the mRNA- and the lipid-containing phases are mainly crucial. Furthermore, the diafiltration volumes and the TMP are significant, as they affect significantly the concentration factor in the SPTFF. These results are in good agreement with the results of the OFAT study (see Figure 11).

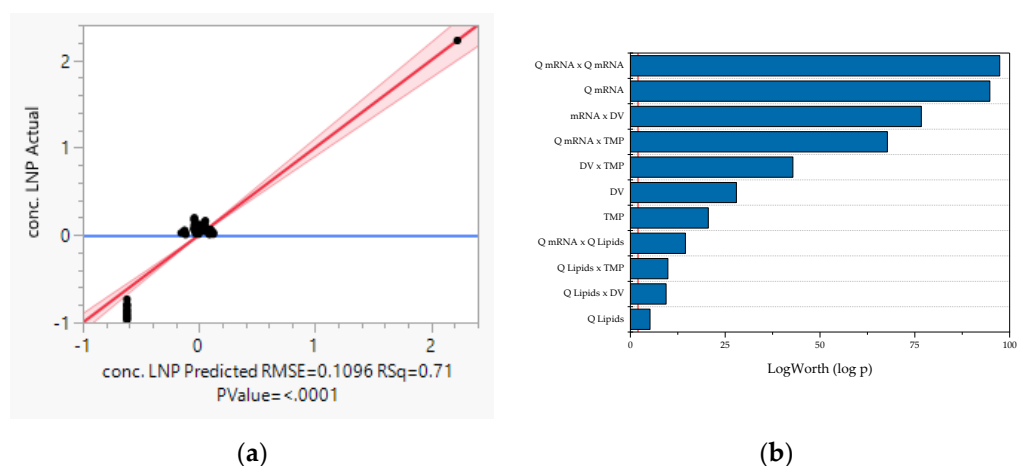


Figure 11. Regression and effect strengths LNP concentration. (a) Actual-vs-predicted plot. (b) log-worth of effects.

Based on the DoE, design spaces can be generated for both target variables (see Figure 12). A condition for the release of the mRNA-LNPs is that the encapsulation efficiency is above 80% [63], which is the case in the green area. From the experimental space studied, it can be seen that, accordingly, the incoming mRNA concentrations must be in a range of approximately 0.26–0.30 g/L. Moreover, this criterion is met when the concentration of PEG lipid is approximately 1.2–1.6 g/L and that of cholesterol is approximately 4.7–6.3 g/L. In addition, the volumetric flow rate of the aqueous buffer should be in the range of 250–295 mL/min.

To obtain maximum LNP concentration, the TMP should be maximum and the diafiltration volumes should be at a value of ten. For the volume flow rate of the mRNA-containing phase, the range around 260 mL/min is ideal. This is within the optimal range for the EE. The color in Figure 13 show low concentrations of LNP (red spectrum) a low DV and TMP in combination with high mRNA flowrate. Toward higher values for TMP (yellow to green) in combination with lower mRNA flowrate, the LNP concentration increases.

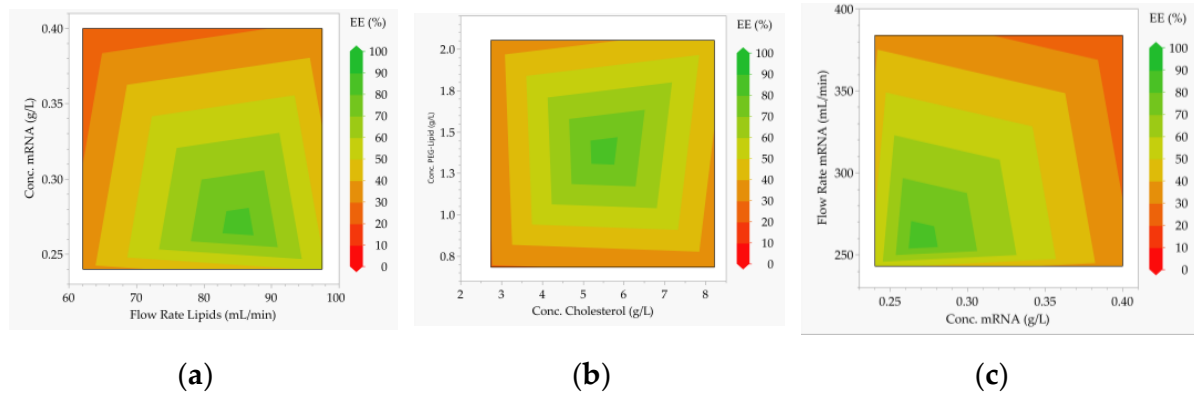


Figure 12. Contour plot LNP encapsulation efficiency. (a) mRNA concentration and flow rate. (b) PEG-lipid concentration and cholesterol concentration. (c) Flow rate and mRNA concentration.

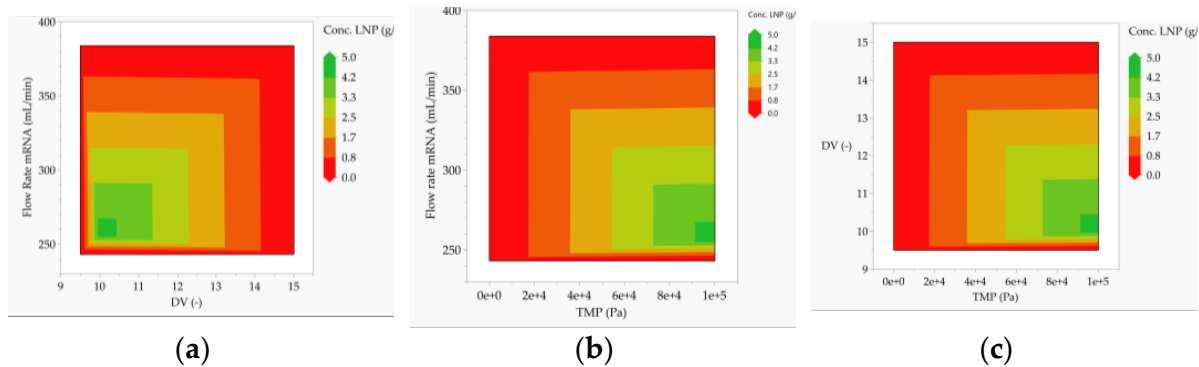
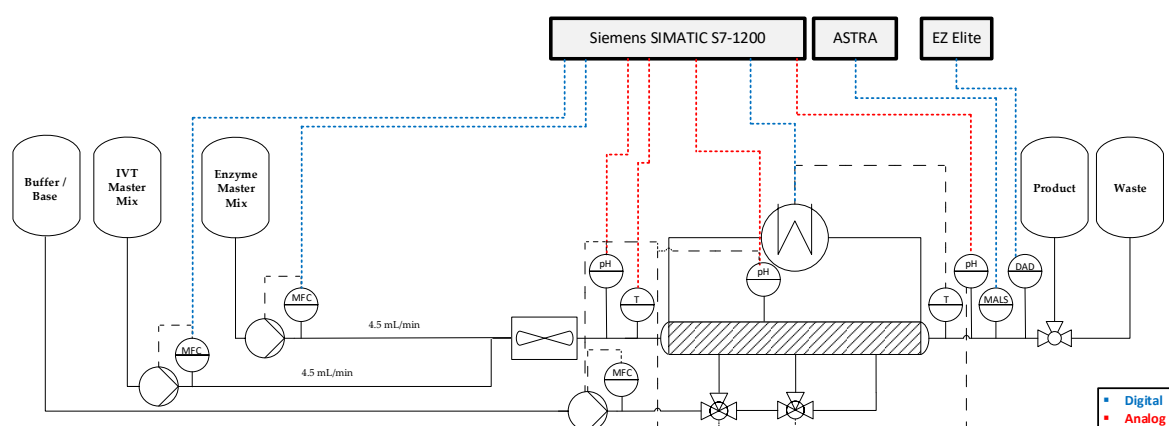


Figure 13. Contour plot LNP concentration. (a) Flow rate and diafiltration volumes. (b) Flow rate and transmembrane pressure. (c) Diafiltration volumes and transmembrane pressure.

3.3. Process Control Strategies

IVT

In vitro transcription takes place in a coiled flow inverter (CFI), the flowsheet of this process step is shown in the Figure 14. The CFI is supplied by two storage tanks containing the master mix with the nucleotides and the master mix with the enzyme. These are each fed by means of a pump at an identical flow rate, which is to be kept constant by means of a mass flow controller (MFC). Both flows are then combined via a dynamic mixer and applied to the reactor. PT100 sensors are located at both the inlet and outlet of the reactor to detect any temperature fluctuations that lead to a loss of enzyme activity. These are compensated by controlling the temperature at the cryostat. In addition to the temperature sensors, pH meters are installed at the inlet and outlet of the reactor as well as at measuring points in the CFI (shown simplified as one sensor in the Figure 14). These detect both pH fluctuations caused by variations in the production of the buffers and the drop in pH due to the reaction. In particular, the latter leads to a loss of enzyme activity of almost 25%, which is why the pH is adjusted by adding base distributed along the length of the reactor. In order to determine the mRNA concentration at the end of the reactor, DAD and MALS/DLS detectors are used, from whose signals the mRNA concentration is determined using PLS models. Based on these results, the volume flow is manipulated by adjusting the pump speed to obtain the optimal residence time and thus the maximum yield.



- Control systems: pH, temperature, mass flow
- Sensors: pH-meters, PT100, mass flow controllers, MALS, DAD

Figure 14. Process flowsheet of IVT.

To simulate the control of the process, the fluctuations in Table 3 were assumed. These result from concentration and pH fluctuations of the purchased substrates as well as fluctuations in the process such as deviating pump speed or temperature deviations. In addition, the drop in pH value due to the reaction is taken into account.

Table 3. Overview of control studies in IVT.

Process Variable	Disturbance	Fluctuation	Control Mechanism
pH	Decrease due to reaction	+0.1/−1	Addition of base/buffer at predefined positions
Temperature	Ambient temperature change	±0.5 °C	Adjust thermostat temperature
Mass Flow	Deviating pump speed	±5%	Adjust pump speed
Master Mix	Deviating concentration(s)	±10%	Adjust volumetric flow rate = residence time

All fluctuations that occurred could be well compensated using PID controllers. In the in vitro transcription, the regulation of the pH value at the first measuring point in the CFI is shown in Figure 15 as an example. Before the control can be performed, the controller must be parameterized. For this purpose, the step response of the system was determined under open-loop condition, as shown in Figure 15, and the parameters were calculated according to Ziegler–Nichols. The integral (T_n) and differential (T_v) parts are very small with 3×10^{-4} min and 7×10^{-5} min, respectively, so they are neglected. The proportional part of the controller is 45%. Figure 15 shows the pH decreasing due to the reaction to a value of about 7.3 (red line), which is regulated back to the optimal pH (setpoint, black line) of 7.9 by adding base (green line). The decrease in pH due to the reaction, which is simulated as a step that is subsequently detected by the pH meter, initializes the addition of base. The addition of base causes the pH to rise locally slightly above the set point. Mixing causes the pH value to settle within the setpoint, so that the optimum pH value can be set within approximately seven seconds.

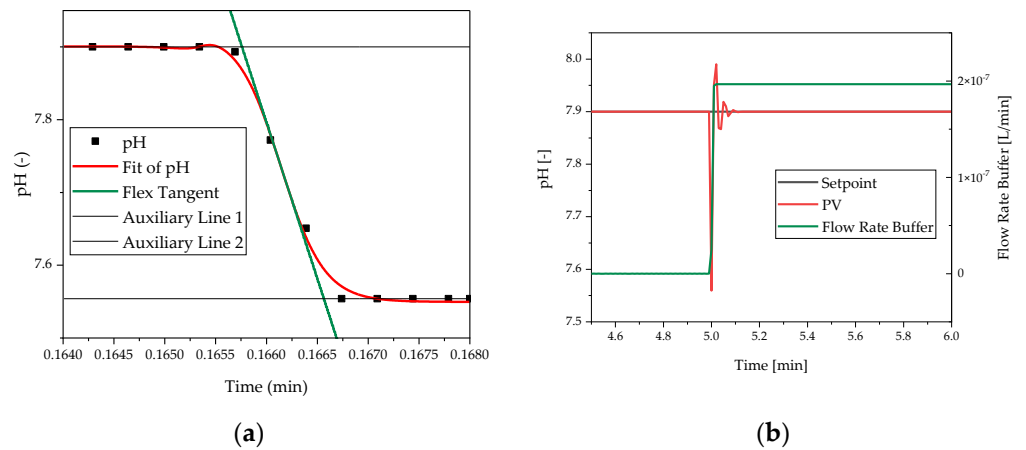


Figure 15. Overview control studies in IVT. (a) Parameter determination. (b) controlled process variable.

Inline Diafiltration by SPTFF

The inline diafiltration process is shown in Figure 16. The feed solution coming from the RPC is set to the target volume flow of 12.1 mL/min by means of a pump and monitored via a mass flow meter. After an inlet pressure transmitter, the product passes through a total of six filtration stages. At each stage, the same amount of exchange buffer is added via a 6-channel pump. The process target is a buffer exchange BE of 99.9% and a VCF of 0.71 to obtain an output concentration of 4.1 g/L. The control sections are shown in blue.

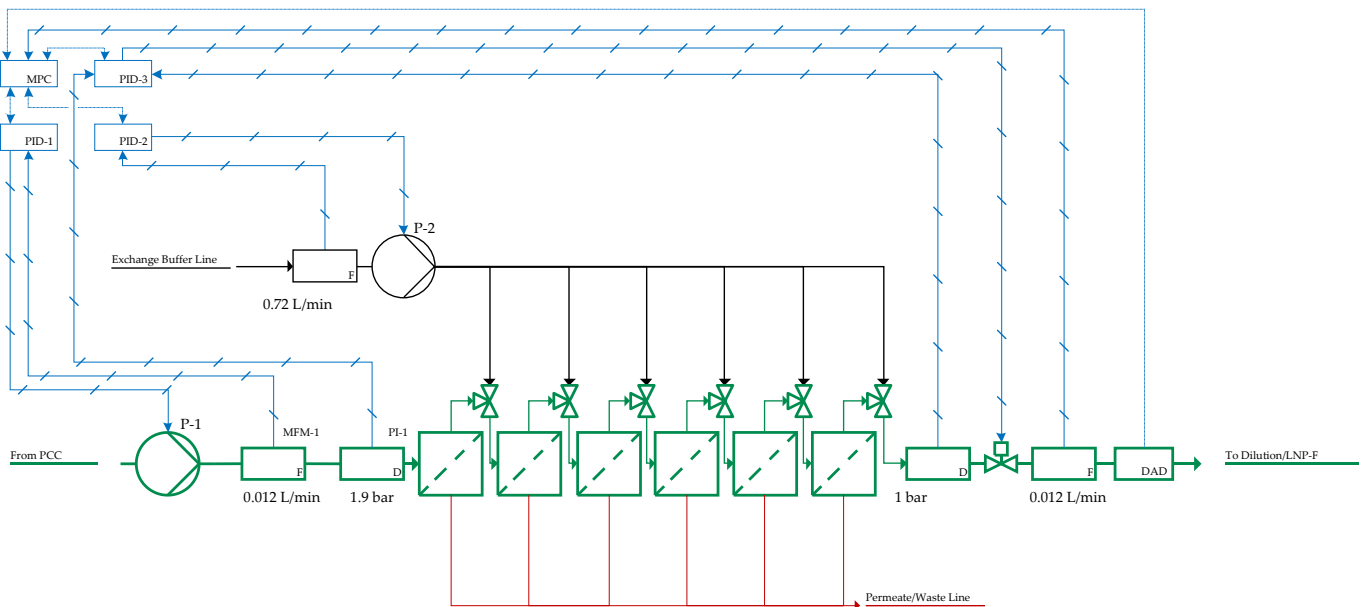


Figure 16. Process flowsheet of inline diafiltration by SPTFF. Green: product stream, blue: sensor signal and actuator control lines to PID and MPC.

A PID controller is used to adjust the retentate valve, which is the setpoint to ensure a constant BE and a constant VCF. Natural pump fluctuations from the setpoint (Table 4) are instantaneously compensated via the mass flow meters, also via PID controllers. Product concentration monitoring via DAD enables RT-QA. Further model-based controls would also be conceivable via this process information, but it is shown that all disturbance cases considered here are feasible for autonomous operation by means of PID controls.

Table 4. Overview control studies in SPTFF.

Process Variable	Disturbance	Fluctuation	Control Mechanism
mRNA	Deviating concentration	$\pm 10\%$	Adjust volumetric flow rate = residence time
Flow Rate Feed	Deviating pump speed	$\pm 5\%$	Adjust pump speed
Flow Rate EB	Deviating pump speed	$\pm 5\%$	Adjust pump speed
Permeate Flux	Decrease due to fouling	$\pm 10\%$	Adjust TMP

Thus, in addition to the natural pump fluctuation, a decrease in permeability due to the increase in filtration resistance can be caused by the control strategy, which, if left unregulated, would lead to a decrease from VCF 0.71 (4.1 g/L) to VCF 0.54 (3.1 g/L) here, as well as an undershoot of the required desalination from 99.9% to 99.6%.

The equalization of these process fluctuations can be compensated within a few minutes both in the case of a longer trend over 180 min and in a failure scenario in which an increase in the membrane resistance is directly caused by unexpected formation of a gel layer (Figure 17).

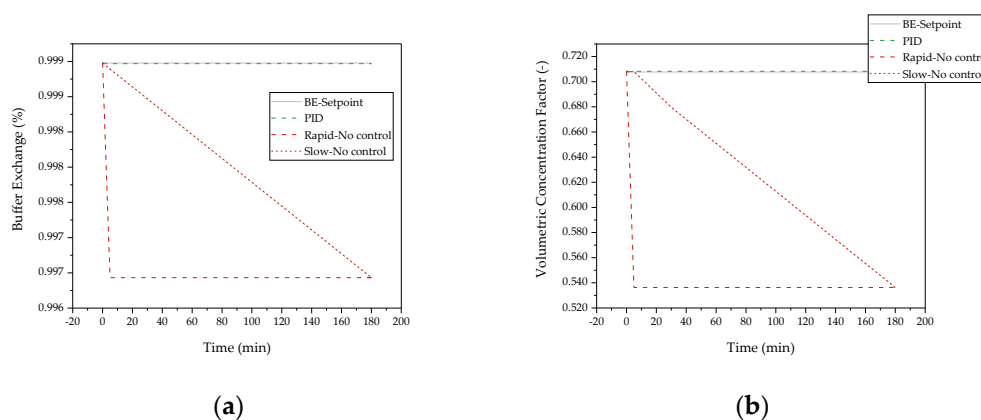
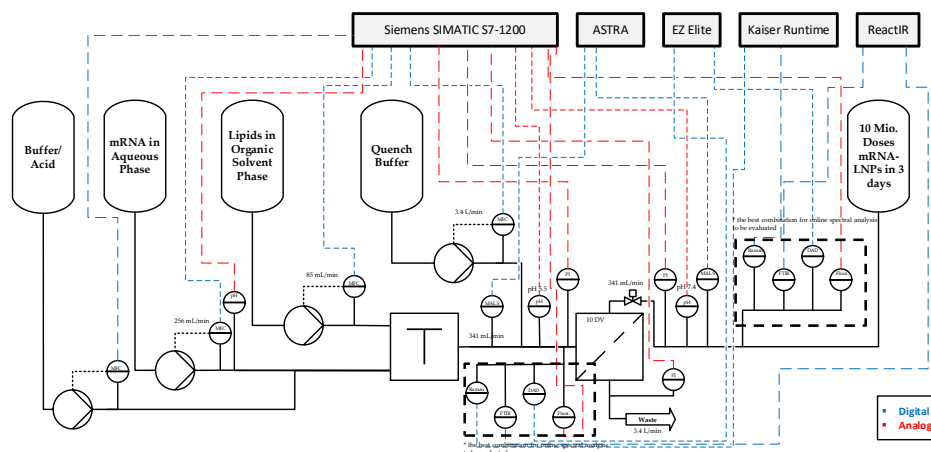


Figure 17. Overview of controlled (green) constant buffer exchange efficiency (left image (a)) respectively VCF (right image (b)) and uncontrolled slow and rapid decrease (dashed red line), when the process is not controlled.

LNP

Figure 18 shows the flowsheet of the LNP formulation, which is divided into two process steps: Mixing in the T-junction mixer and subsequent quenching of the reaction via diafiltration in the SPTFF. In the T-junction mixer, the mRNA-containing aqueous phase is rapidly mixed in a 3:1 ratio with the lipid-containing organic solvent phase. The two buffers are fed to the mixer via one pump each, with the volume flows controlled by one MFC each. The aqueous buffer has a pH of four, so that a pH of about 5.5 is obtained during mixing. This is below the pKa value of the ionizable lipid [64], as a result of which it is ionized and thus positively charged. Accordingly, both the pH of the aqueous buffer and the pH at the outlet of the mixer are measured and, if necessary, adjusted by adding acid to the mRNA-containing phase to ensure that ionization can occur. The second process step involves quenching the reaction by performing a diafiltration with ten diafiltration volumes of PBS in a SPTFF. This is performed by connecting several hollow fiber modules in series, which is simplified in the flowsheet as one filtration module. The aim of diafiltration is to increase the pH and thus neutralize the lipid and stop the reaction so that LNPs of defined size can be formed. Furthermore, diafiltration has the purpose of removing the organic solvent phase. For this task, Quench Buffer is added via a pump and the volume flow rate is controlled via an MFC to ensure the addition of sufficient diafiltration volumes for pH adjustment and buffer exchange. To set the optimal TMP, pressure sensors are used in the feed, permeate, and retentate streams. In order to be able

to determine the product properties such as LNP concentration, size and encapsulation efficiency continuously during the process, various PAT detectors are used. These include in particular the MALS/DLS. In addition, Raman and FTIR spectrometers as well as DAD and fluorescence detectors are used, although the determination of the best combination of detectors for online spectral analysis is still pending. PLS models can then be used to draw conclusions about the product properties from the measured signals and, if necessary, to adjust the pump speed of the aqueous or organic phase to ensure an optimum residence time in the mixer and the SPTFF.



- Control systems: pH, mass flow, TMP
- Sensors: pH-meters, mass flow controllers, pressure indicators, MALS, Raman, FTIR, DAD, Fluorescence

Figure 18. LNP process flow sheet.

To simulate the control of the process, the fluctuations in Table 5 were assumed. These result from concentration and pH fluctuations of the purchased substrates as well as fluctuations in the process such as deviating pump speed or fluctuations in previous process steps. Furthermore, the permeate flux decrease due to fouling.

Table 5. Overview control studies in LNP.

Process Variable	Disturbance	Fluctuation	Control Mechanism
mRNA	Deviating concentration	±10%	Adjust volumetric flow rate = residence time
pH aq. buffer	Deviating value	±0.2	Addition of acid/buffer
Lipids	Deviating concentration(s)	±5%	Adjust volumetric flow rate = residence time
Flow Rate	Deviating pump speed	±5%	Adjust pump speed
Dv	Deviating pump speed	±5%	Adjust pump speed
Permeate Flux	Decrease due to fouling	±10%	Adjust TMP

All occurring fluctuations could be well compensated by means of a PID controller. The controller was designed open-loop by determining the step response of the system. Subsequently, the parameters were determined according to Ziegler–Nichols. Figure 19 shows an example of the control of the volumetric flow rate of the aqueous buffer. For the control task, it was assumed that the pump speed and the mRNA concentration jump simultaneously. This reduces the residence time in which the encapsulation reaction of mRNA can occur. Consequently, the encapsulation efficiency decreases. After evaluating the step response, the proportional component is found to be 0.8%, the integral component is 12 s, and the differential component is 3 s. After the sharp loss of EE has been registered

by the PAT detector, the volumetric flow rate of the aqueous buffer is reduced to increase the residence time and thus the encapsulation efficiency. This allows the loss of EE to be reduced by 86% to only 0.2% within 2.6 min.

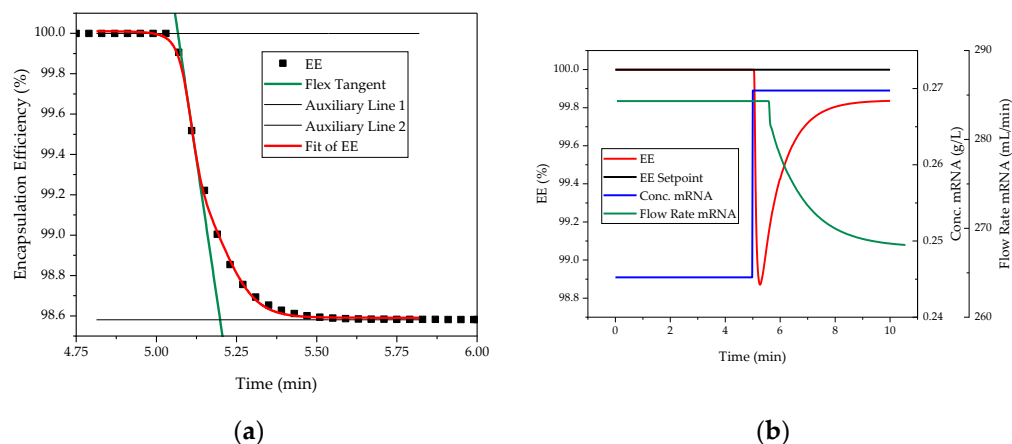


Figure 19. Overview control studies in LNP. (a) Parameter determination. (b) controlled process variable.

4. Conclusions

Digital twins support accelerated process design and development [13,65–68] up to basic and detail engineering including process control system configuration and enable among others an operator training simulator in combination with the existing process control system, and are a well-established and beneficial procedure in petro-, basic-, and fine-chemicals industry. Moreover, operator workload is reduced drastically, as they are enabled of operating different plants in parallel—a most wanted capacity increase option at enhanced product robustness [32]. Digital-twin based process automation reduces the number of operators required by factor of two and lowers their workload and even stress level drastically [69]. In addition, product quality is subject to less fluctuation due to the continuous production method and the steady-state thus ensured, which has a lower time-to-market due to PAT-supported RTRT as well as lower batch failure rates which enlarges productivity in case of mRNA manufacturing by about 20% [69].

It was shown that manufacturing costs could be reduced to about 25% (factor of four) by continuous in vitro transcription. The largest savings can be achieved by reducing personnel and consumables per campaign; in the semi-continuous case, a reduction in consumable costs by a factor of six and a reduction in personnel efforts (proportional to costs) by a factor of 20 is possible. In the fully continuous case, savings of a factor of 7.5 (consumables) and a factor of 30 (personnel) can be achieved. Due to the significant share of raw materials in the manufacturing costs (74–97%), these factors are not reflected proportionally in the manufacturing costs. If a recycling strategy for the most cost-intensive starting materials (T7 RNA polymerase and cap analog), which has already been discussed in the literature, is implemented, the raw material costs can be reduced by a factor of about four. Combining the above cost reduction approaches leads to a potential reduction in manufacturing costs by a factor of about five (i.e., from EUR 0.380 per dose to EUR 0.085 per dose) [32,69].

This points out the specific competitiveness of the whole continuous biomanufacturing approach based on consistent industrialization of digital twins. Moreover, the QbD-based process control design with aid of digital twins for the whole process proves the statement that industrialization of an autonomous continuous mRNA vaccine manufacturing platform is directly based on standard clever PID controller on hand. Additional advanced process control approaches are recommended to be based on the already existing digital twins as model-based predictive control integration of the available PAT strategies [70–72]. Potential improvement of addition about 15–20% productivity increasement and person-

nel as well as chemicals reduction of about 30% could be predicted with the simulation studies evaluated [40]. While discussing efforts and benefits it should be kept in mind that autonomous operation is a key technology for any decentral local container-based manufacturing concept in the future [73,74] as those approaches are only feasible without skilled operators transferred abroad but less local manpower and remote access sophisticated support by the main manufacturer. Efficient and fast worldwide mRNA therapeutics supply at lowest cost and resources is technically feasible for industrialization.

Author Contributions: A.S. was responsible for filtration studies; H.H. and A.H. were responsible for studies regarding IVT; S.Z.-R. and F.L.V. were responsible for simulation of chromatographic separation; A.H. was also responsible for LNP studies; J.S. substantively revised the work and contributed the materials and analysis tools; J.S. is responsible for the conception and supervision. All authors have read and agreed to the published version of the manuscript.

Funding: The authors acknowledge financial support by Open Access Publishing Fund of Clausthal University of Technology.

Institutional Review Board Statement: Not applicable.

Informed Consent Statement: Not applicable.

Data Availability Statement: Not applicable.

Acknowledgments: The authors would like to acknowledge their institute's laboratory colleagues, especially Frank Steinhäuser and Volker Strohmeyer as well as the PCS team Thomas Knebel with Christian Siemers, Automation Technology, and Christian Bohn, Control Engineering, at Clausthal University of Technology.

Conflicts of Interest: The authors declare no conflict of interest.

References

1. Melinek, B.; Colant, N.; Stamatis, C.; Lennon, C.; Farid, S.S.; Polizzi, K.; Carver, M.; Bracewell, D.G. Toward a Roadmap for Cell-Free Synthesis in Bioprocessing. Available online: <https://bioprocessintl.com/upstream-processing/expression-platforms/toward-a-roadmap-for-cell-free-synthesis-in-bioprocessing/> (accessed on 2 March 2021).
2. Ipsen Biopharm Ltd. Novel Production Process for a Highly Potent Recombinant Protein Using Doggybone DNA (dbDNA) Vector and Cell Free Expression Technology. 2020. Available online: <https://gtr.ukri.org/projects?ref=104201> (accessed on 3 June 2021).
3. GenScript ProBio. Accelerating Vaccine Development against COVID-19. 2020. Available online: https://www.genscriptprobio.com/gsfiles/techfiles/GPB-COVID19-GMP%20plasmid-GPB_052020.pdf (accessed on 6 March 2021).
4. Shin, D.; Azizian, K.T.; Henderson, J.M.; Hogrefe, R.I.; Lebedev, A.; Houston, M.; McCaffrey, A.P. CleanCap@Co-transcriptional Capping Streamlines mRNA Manufacturing. Available online: https://www.trilinkbiotech.com/media/contentmanager/content/mRNA_WVC2_1.pdf (accessed on 6 March 2021).
5. Whitley, J.; Zwolinski, C.; Denis, C.; Maughan, M.; Hayles, L.; Clarke, D.; Snare, M.; Liao, H.; Chiou, S.; Marmura, T.; et al. Development of mRNA manufacturing for vaccines and therapeutics: mRNA platform requirements and development of a scalable production process to support early phase clinical trials. *Transl. Res.* **2022**, *242*, 38–55. [CrossRef] [PubMed]
6. Weise, E.; Weintraub, K. A COVID-19 Vaccine Life Cycle: From DNA to Doses. 2021. Available online: <https://eu.usatoday.com/in-depth/news/health/2021/02/07/how-covid-vaccine-made-step-step-journey-pfizer-dose/4371693001/> (accessed on 6 March 2021).
7. von der Mülbe, F.; Reidel, L.; Ketterer, T.; Gontcharova, L.; Bauer, S.; Pascolo, S.; Probst, J.; Schmid, A. Method for Producing RNA. Available online: <https://patents.google.com/patent/US10017826B2/en> (accessed on 3 August 2022).
8. BIA Separations. Purification of mRNA with CIMmultus PrimaS™: Technical Note. 2020. Available online: <https://www.biaseparations.com/en/library/technical-notes/1088/purification-of-mrna-with-cimmultus-primastm> (accessed on 2 March 2021).
9. Nemeč, K.S.; Cernigoj, U.; Vidic, J.; Livk, A.G.; Goricar, B.; Božic, K.; Celjar, A.M.; Skok, J.; Mencin, N.; Kralj, S.; et al. High Yield mRNA Production Process from E. coli to Highly Pure mRNA. 2020. Available online: <https://www.biaseparations.com/en/library/seminars-webinars/1098/high-yield-mrna-production-process-from-ecoli-to-highly-pure-mrna> (accessed on 2 March 2021).
10. Zobel-Roos, S.; Stein, D.; Strube, J. Evaluation of Continuous Membrane Chromatography Concepts with an Enhanced Process Simulation Approach. *Antibodies* **2018**, *7*, 13. [CrossRef] [PubMed]
11. *Ullmann's Encyclopedia of Industrial Chemistry*; Wiley-VCH Verlag GmbH & Co. KGaA: Weinheim, Germany, 2000; ISSN 3527306730.

12. Vetter, F.L.; Zobel-Roos, S.; Mota, J.P.; Nilsson, B.; Schmidt, A.; Strube, J. Toward Autonomous Production of mRNA-Therapeutics in the Light of Advanced Process Control and Traditional Control Strategies for Chromatography: Submitted. *Processes* **2022**.
13. Vetter, F.L.; Strube, J. Enabling Total Process Digital Twin in Sugar Refining through the Integration of Secondary Crystallization Influences. *Processes* **2022**, *10*, 373. [[CrossRef](#)]
14. Helling, C.; Strube, J. Quality-by-Design with Rigorous Process Modeling as Platform Technology of the Future. *Chem. Ing. Tech.* **2012**, *84*, 1334. [[CrossRef](#)]
15. Yu, L.X.; Amidon, G.; Khan, M.A.; Hoag, S.W.; Polli, J.; Raju, G.K.; Woodcock, J. Understanding pharmaceutical quality by design. *AAPS J.* **2014**, *16*, 771–783. [[CrossRef](#)]
16. Uhlenbrock, L.; Sixt, M.; Strube, J. Quality-by-Design (QbD) process evaluation for phytopharmaceuticals on the example of 10-deacetylbaicatin III from yew. *Resour.-Effic. Technol.* **2017**, *3*, 137–143. [[CrossRef](#)]
17. Zobel-Roos, S.; Schmidt, A.; Mestmäcker, F.; Mouellef, M.; Huter, M.; Uhlenbrock, L.; Kornecki, M.; Lohmann, L.; Ditz, R.; Strube, J. Accelerating Biologics Manufacturing by Modeling or: Is Approval under the QbD and PAT Approaches Demanded by Authorities Acceptable Without a Digital-Twin? *Processes* **2019**, *7*, 94. [[CrossRef](#)]
18. ICH Expert Working Group. PHARMACEUTICAL DEVELOPMENT Q8(R2). In Ich Harmonised Tripartite Guideline; 2009; pp. 1–28. Available online: https://database.ich.org/sites/default/files/Q8_R2_Guideline.pdf (accessed on 3 August 2022).
19. ICH Expert Working Group. Quality risk management Q9, Current step. In Ich Harmonised Tripartite Guideline; 2005; p. 408. Available online: <https://educationfactory.de/wp-content/uploads/2020/05/ICH-Q9-Quality-Risk-Management.pdf> (accessed on 3 August 2022).
20. ICH Expert Working Group. Pharmaceutical quality system Q10. In Ich Harmonised Tripartite Guideline; 2008. Available online: <https://www.cls.co.at/media/files/ich-q10---pharmaceutial-quality-system.pdf> (accessed on 3 August 2022).
21. ICH Expert Working Group. Development and manufacture of drug substances (chemical entities and biotechnological/biological entities) Q11. In Ich Harmonised Tripartite Guideline; 2011. Available online: <http://www.nihs.go.jp/dbcb/TEXT/Q11.pdf> (accessed on 3 August 2022).
22. Alt, N.; Zhang, T.Y.; Motchnik, P.; Taticek, R.; Quarmby, V.; Schlothauer, T.; Beck, H.; Emrich, T.; Harris, R.J. Determination of critical quality attributes for monoclonal antibodies using quality by design principles. *Biologicals* **2016**, *44*, 291–305. [[CrossRef](#)]
23. Sixt, M.; Uhlenbrock, L.; Strube, J. Toward a Distinct and Quantitative Validation Method for Predictive Process Modelling—On the Example of Solid-Liquid Extraction Processes of Complex Plant Extracts. *Processes* **2018**, *6*, 66. [[CrossRef](#)]
24. Steinebach, F.; Angarita, M.; Karst, D.J.; Müller-Späth, T.; Morbidelli, M. Model based adaptive control of a continuous capture process for monoclonal antibodies production. *J. Chromatogr. A* **2016**, *1444*, 50–56. [[CrossRef](#)]
25. Steinebach, F.; Müller-Späth, T.; Morbidelli, M. Continuous counter-current chromatography for capture and polishing steps in biopharmaceutical production. *Biotechnol. J.* **2016**, *11*, 1126–1141. [[CrossRef](#)] [[PubMed](#)]
26. Steinebach, F.; Ulmer, N.; Wolf, M.; Decker, L.; Schneider, V.; Wälchli, R.; Karst, D.; Souquet, J.; Morbidelli, M. Design and operation of a continuous integrated monoclonal antibody production process. *Biotechnol. Prog.* **2017**, *33*, 1303–1313. [[CrossRef](#)] [[PubMed](#)]
27. Kornecki, M.; Schmidt, A.; Lohmann, L.; Huter, M.; Mestmäcker, F.; Klepzig, L.; Strube, J. Accelerating Biomanufacturing by Modeling of Continuous Bioprocessing—Piloting Case Study of Monoclonal Antibody Manufacturing. *Processes* **2019**, *7*, 495. [[CrossRef](#)]
28. Helgers, H.; Schmidt, A.; Lohmann, L.J.; Vetter, F.L.; Juckers, A.; Jensch, C.; Mouellef, M.; Zobel-Roos, S.; Strube, J. Towards Autonomous Operation by Advanced Process Control—Process Analytical Technology for Continuous Biologics Antibody Manufacturing. *Processes* **2021**, *9*, 172. [[CrossRef](#)]
29. Geering, H.P. *Regelungstechnik: Mathematische Grundlagen, Entwurfsmethoden, Beispiele*; Springer: Berlin/Heidelberg, Germany, 1994; ISBN 978-3-662-09719-9.
30. Armstrong, A.; Horry, K.; Cui, T.; Hulley, M.; Turner, R.; Farid, S.S.; Goldrick, S.; Bracewell, D.G. Advanced control strategies for bioprocess chromatography: Challenges and opportunities for intensified processes and next generation products. *J. Chromatogr. A* **2021**, *1639*, 461914. [[CrossRef](#)]
31. Nordh, P. Understand Advanced Process Control. Available online: <https://www.aiche.org/resources/publications/cep/2016/june/understand-advanced-process-control> (accessed on 29 June 2021).
32. Schmidt, A.; Helgers, H.; Vetter, F.L.; Juckers, A.; Strube, J. Digital Twin of mRNA-Based SARS-COVID-19 Vaccine Manufacturing towards Autonomous Operation for Improvements in Speed, Scale, Robustness, Flexibility and Real-Time Release Testing. *Processes* **2021**, *9*, 748. [[CrossRef](#)]
33. Zobel-Roos, S.; Schmidt, A.; Uhlenbrock, L.; Ditz, R.; Köster, D.; Strube, J. Digital Twins in Biomanufacturing. *Adv. Biochem. Eng. Biotechnol.* **2021**, *176*, 181–262. [[CrossRef](#)]
34. Nikita, S.; Thakur, G.; Jesubalan, N.G.; Kulkarni, A.; Yezhuvath, V.B.; Rathore, A.S. AI-ML applications in bioprocessing: ML as an enabler of real time quality prediction in continuous manufacturing of mAbs. *Comput. Chem. Eng.* **2022**, *164*, 107896. [[CrossRef](#)]
35. Mouellef, M.; Szabo, G.; Vetter, F.L.; Siemers, C.; Strube, J. Artificial Neural Network for Fast and Versatile Model Parameter Adjustment Utilizing PAT Signals of Chromatography Processes for Process Control under Production Conditions. *Processes* **2022**, *10*, 709. [[CrossRef](#)]
36. Kornecki, M.; Strube, J. Process Analytical Technology for Advanced Process Control in Biologics Manufacturing with the Aid of Macroscopic Kinetic Modeling. *Bioengineering* **2018**, *5*, 25. [[CrossRef](#)] [[PubMed](#)]

37. Schmidt, A.; Helgers, H.; Lohmann, L.J.; Vetter, F.; Juckers, A.; Mouellef, M.; Zobel-Roos, S.; Strube, J. Process analytical technology as key-enabler for digital twins in continuous biomanufacturing. *J. Chem. Technol. Biotechnol.* **2022**. [[CrossRef](#)]
38. Juckers, A.; Knerr, P.; Harms, F.; Strube, J. Advanced Process Analytical Technology in Combination with Process Modeling for Endpoint and Model Parameter Determination in Lyophilization Process Design and Optimization. *Processes* **2021**, *9*, 1600. [[CrossRef](#)]
39. Hengelbrock, A.; Helgers, H.; Schmidt, A.; Vetter, F.L.; Juckers, A.; Rosengarten, J.F.; Stitz, J.; Strube, J. Digital Twin for HIV-Gag VLP Production in HEK293 Cells. *Processes* **2022**, *10*, 866. [[CrossRef](#)]
40. Helgers, H.; Hengelbrock, A.; Schmidt, A.; Strube, J. Digital Twins for Continuous mRNA Production. *Processes* **2021**, *9*, 1967. [[CrossRef](#)]
41. Zobel-Roos, S.; Mouellef, M.; Siemers, C.; Strube, J. Process Analytical Approach towards Quality Controlled Process Automation for the Downstream of Protein Mixtures by Inline Concentration Measurements Based on Ultraviolet/Visible Light (UV/VIS) Spectral Analysis. *Antibodies* **2017**, *6*, 24. [[CrossRef](#)]
42. Kornecki, M.; Schmidt, A.; Strube, J. PAT as key-enabling technology for QbD in pharmaceutical manufacturing A conceptual review on upstream and downstream processing. *Chim. Oggi-Chem. Today* **2018**, *36*, 44–48.
43. Vetter, F.L.; Zobel-Roos, S.; Strube, J. PAT for Continuous Chromatography Integrated into Continuous Manufacturing of Biologics towards Autonomous Operation. *Processes* **2021**, *9*, 472. [[CrossRef](#)]
44. Lohmann, L.J.; Strube, J. Process Analytical Technology for Precipitation Process Integration into Biologics Manufacturing towards Autonomous Operation—mAb Case Study. *Processes* **2021**, *9*, 488. [[CrossRef](#)]
45. Arnold, S.; Siemann, M.; Scharnweber, K.; Werner, M.; Baumann, S.; Reuss, M. Kinetic modeling and simulation of in vitro transcription by phage T7 RNA polymerase. *Biotechnol. Bioeng.* **2001**, *72*, 548–561. [[CrossRef](#)]
46. Kartje, Z.J.; Janis, H.I.; Mukhopadhyay, S.; Gagnon, K.T. Revisiting T7 RNA polymerase transcription in vitro with the Broccoli RNA aptamer as a simplified real-time fluorescent reporter. *J. Biol. Chem.* **2021**, *296*, 100175. [[CrossRef](#)] [[PubMed](#)]
47. Bhagavan, N.V. Water, Acids, Bases, and Buffers. In *Medical Biochemistry*; Elsevier: Amsterdam, The Netherlands, 2002; pp. 1–16. ISBN 9780120954407.
48. Taylor, G. Dispersion of soluble matter in solvent flowing slowly through a tube. *Proc. R. Soc. Lond. A* **1953**, *219*, 186–203. [[CrossRef](#)]
49. Danckwerts, P.V. *Continuous Flow Systems*; Elsevier: Amsterdam, The Netherlands, 1953.
50. Kovo, A.S. Mathematical Modeling and Simulation of Dispersion in a Nonideal Plug Flow Reactor. *J. Dispers. Sci. Technol.* **2008**, *29*, 1129–1134. [[CrossRef](#)]
51. Huter, M.J.; Jensch, C.; Strube, J. Model Validation and Process Design of Continuous Single Pass Tangential Flow Filtration Focusing on Continuous Bioprocessing for High Protein Concentrations. *Processes* **2019**, *7*, 781. [[CrossRef](#)]
52. Huter, M.J.; Strube, J. Model-Based Design and Process Optimization of Continuous Single Pass Tangential Flow Filtration Focusing on Continuous Bioprocessing. *Processes* **2019**, *7*, 317. [[CrossRef](#)]
53. Huter, M.J. Modellunterstützte Prozessauslegung Unterschiedlicher Grundoperationen am Beispiel von Kontinuierlicher Ultrafiltration und absatzweiser Kristallisation. Doctor Thesis, Clausthal University of Technology, Clausthal, Germany, 2021.
54. Thiess, H.; Leuthold, M.; Grummert, U.; Strube, J. Module design for ultrafiltration in biotechnology: Hydraulic analysis and statistical modeling. *J. Membr. Sci.* **2017**, *540*, 440–453. [[CrossRef](#)]
55. Thiess, H. Modellierung von Membrantrennverfahren am Beispiel der Ultrafiltration in der Biotechnologischen und der Pervaporation in der Chemischen Verfahrenstechnik. Doctor Thesis, Clausthal University of Technology, Clausthal, Germany, 2019.
56. Michaels, A.S. New separation technique for CPI. *Chem. Eng. Prog.* **1968**, *64*, 31.
57. Food and Drug Administration. Pfizer-BioNTech COVID-19 Vaccine EUA Letter of Authorization Reissued 05-10-2021. Available online: <https://www.fda.gov/media/144412/download> (accessed on 3 August 2022).
58. Avery, H.E. *Basic Reaction Kinetics and Mechanisms*; Macmillan: London, UK, 1974; ISBN 0333126963.
59. Drake, P.L.; Hartshorn, R.T.; McGinnis, J.; Sykes, A.G. pH dependence of rate constants for reactions of cytochrome c with inorganic redox partners and mechanistic implications. *Inorg. Chem.* **1989**, *28*, 1361–1366. [[CrossRef](#)]
60. Ziegler, J.G.; Nichols, N.B. Optimum Settings for Automatic Controllers. *J. Dyn. Syst. Meas. Control.* **1993**, *115*, 220–222. [[CrossRef](#)]
61. Zacher, S.; Reuter, M. *Regelungstechnik für Ingenieure*; Springer Fachmedien Wiesbaden: Wiesbaden, Germany, 2017; ISBN 978-3-658-17631-0.
62. Chien, K.L.; Hrones, J.A.; Reswick, J.B. On the Automatic Control of Generalized Passive Systems. *Trans. Am. Soc. Mech. Eng.* **1952**, *74*, 175–185. [[CrossRef](#)]
63. Daniel, S.; Kis, Z.; Kontoravdi, C.; Shah, N. Quality by Design for enabling RNA platform production processes. *Trends Biotechnol.* **2022**. [[CrossRef](#)] [[PubMed](#)]
64. Buschmann, M.D.; Carrasco, M.J.; Alishetty, S.; Paige, M.; Alameh, M.G.; Weissman, D. Nanomaterial Delivery Systems for mRNA Vaccines. *Vaccines* **2021**, *9*, 65. [[CrossRef](#)] [[PubMed](#)]
65. Uhlenbrock, L.; Jensch, C.; Tegtmeier, M.; Strube, J. Digital Twin for Extraction Process Design and Operation. *Processes* **2020**, *8*, 866. [[CrossRef](#)]
66. Lohmann, L.J.; Strube, J. Accelerating Biologics Manufacturing by Modeling: Process Integration of Precipitation in mAb Downstream Processing. *Processes* **2020**, *8*, 58. [[CrossRef](#)]

67. Mouellef, M.; Vetter, F.L.; Zobel-Roos, S.; Strube, J. Fast and Versatile Chromatography Process Design and Operation Optimization with the Aid of Artificial Intelligence. *Processes* **2021**, *9*, 2121. [[CrossRef](#)]
68. Klepzig, L.S.; Juckers, A.; Knerr, P.; Harms, F.; Strube, J. Digital Twin for Lyophilization by Process Modeling in Manufacturing of Biologics. *Processes* **2020**, *8*, 1325. [[CrossRef](#)]
69. Schmidt, A.; Helgers, H.; Vetter, F.L.; Juckers, A.; Strube, J. Fast and Flexible mRNA Vaccine Manufacturing as a Solution to Pandemic Situations by Adopting Chemical Engineering Good Practice—Continuous Autonomous Operation in Stainless Steel Equipment Concepts. *Processes* **2021**, *9*, 1874. [[CrossRef](#)]
70. Helgers, H.; Schmidt, A.; Strube, J. Towards Autonomous Process Control—Digital Twin for CHO Cell-Based Antibody Manufacturing Using a Dynamic Metabolic Model. *Processes* **2022**, *10*, 316. [[CrossRef](#)]
71. Helgers, H.; Hengelbrock, A.; Schmidt, A.; Rosengarten, J.; Stitz, J.; Strube, J. Process Design and Optimization towards Digital Twins for HIV-Gag VLP Production in HEK293 Cells, including Purification. *Processes* **2022**, *10*, 419. [[CrossRef](#)]
72. Helgers, H.; Hengelbrock, A.; Schmidt, A.; Vetter, F.L.; Juckers, A.; Strube, J. Digital Twins for scFv Production in *Escherichia coli*. *Processes* **2022**, *10*, 809. [[CrossRef](#)]
73. Saied, A.A.; Metwally, A.A.; Dhawan, M.; Choudhary, O.P.; Aiash, H. Strengthening vaccines and medicines manufacturing capabilities in Africa: Challenges and perspectives. *EMBO Mol. Med.* **2022**, *14*, e16287. [[CrossRef](#)] [[PubMed](#)]
74. Uli Beisel. BioNTainer—A Manufacturing Solution for Africa or Circumventing Capacity? Available online: <https://www.medizinethnologie.net/biontainer-a-manufacturing-solution-for-africa-or-circumventing-capacity/> (accessed on 1 August 2022).